Statistical Osteoporosis Models Using Composite Finite Elements: A Parameter Study

Uwe Wolfram[*]   Lars Ole Schwen[†]   Ulrich Simon[*]

Martin Rumpf[†]   Hans-Joachim Wilke[*]

Osteoporosis is a widely spread disease with severe consequences for patients and high costs for health care systems. The disease is characterised by a loss of bone mass which induces a loss of mechanical performance and structural integrity. It was found that transverse trabeculae are thinned and perforated while vertical trabeculae stay intact. For understanding these phenomena and the mechanisms leading to fractures of trabecular bone due to osteoporosis, numerous researchers employ micro-finite element models. To avoid disadvantages in setting up classical finite element models, composite finite elements (CFE) can be used.

The aim of the study is to test the potential of CFE. For that, a parameter study on numerical lattice samples with statistically simulated, simplified osteoporosis is performed. These samples are subjected to compression and shear loading.

Results show that the biggest drop of compressive stiffness is reached for transverse isotropic structures losing 32% of the trabeculae (minus 89.8% stiffness). The biggest drop in shear stiffness is found for an isotropic structure also losing 32% of the trabeculae (minus 67.3% stiffness).

The study indicates that losing trabeculae leads to a worse drop of macroscopic stiffness than thinning of trabeculae. The results further demonstrate the advantages of CFEs for simulating micro-structured samples.

Keywords: micro finite element models, composite finite elements, trabecular bone, statistical osteoporosis

AMS Subject Classifications: 74S05, 74B05

[*]Institute of Orthopaedic Research and Biomechanics, Ulm University.
  Corresponding author: Uwe Wolfram, Helmholtzstraße 14, 89081 Ulm, Germany.
  Phone: +49 731 55301, Fax: +49 731 55302, e-mail: `uwe.wolfram@uni-ulm.de`
[†]Institute for Numerical Simulation, University of Bonn

1 Introduction

Osteoporosis is a widely spread disease [RSN+95] characterised by a loss of bone mass which induces a loss of stiffness and structural integrity [KOJ05, MM01].

Numerous researchers investigated the mechanical properties of trabecular bone using voxel-based micro finite element models (μFE) models [MHR94, GK02, vRHER03, MYK05, TWV+06, WWKL07, CPA+07]. Direct conversion of voxels gained from computed tomography into a hexahedral FE mesh is a robust method but results in a rough mesh with nonsmooth surfaces. Subsequent smoothing [BM06] can lead to distorted elements and thus possibly to a corruption of the results. Generating "good" tetrahedral meshes is a nontrivial problem [BE92, TW00, She02]. Moreover, they are inherently unstructured. This prohibits the application of geometric multigrid methods [Bra77, Xu89, BR02] for efficient numerical computation.

To overcome these disadvantages in classical μFE models, composite finite elements (CFE) introduced in [HS97b, HS97a, HS98] can be used. A 3D implementation in case of an image based domain description is presented in [LPR+09, PRS07].

In contrast to μFE models of trabecular structures, [YK99, GK02, DSG05, DSMG07] proposed lattice models to simulate osteoporotic and nonosteoporotic trabecular bone by varying trabecular thickness, spacing or random material removal. Compared to lattice models, the volume-based CFE approach permits a much better resolution of the elastic behaviour at trabecular crossings.

This study aims to test the potential of CFE on parameter studies on artificial lattice samples with statistically simulated, simplified osteoporosis. These samples are meant to investigate the influence of structural changes, such as degradation or thinning of trabeculae on the macroscopic stiffness, being one influence factor (among others) on biomechanical stability.

2 Materials and Methods

2.1 Geometries of Samples

We consider artificial micro-structured, elastic specimens consisting of equidistant $10 \times 10 \times 10$ rods with circular cross section with diameter $d = 0.134$ mm [HLM+99] and length $l = 0.335$ mm for the starting configuration. These specimens represent one cell of a periodic micro-structure big enough for determining macroscopic material parameters [HJMH88].

Displacement boundary conditions are applied to all free trabecular ends on two opposite faces of the bounding box: The bottom face is clamped so that the displacement is zero. The top face is loaded separately with a displacement in longitudinal direction (compression in z) or in a transverse direction (shear in x), both by 1% of the edge length of the sample. We do not impose displacement boundary conditions on the remaining four side faces.

All trabeculae in one space direction have the same diameter, so the sample is fully described by triples of trabecular diameter-to-length ratios d/l. Similarly, the entries of the degradation ratio triples p specify the ratio of trabeculae (up to integer rounding) randomly removed in each space direction.

2.2 Composite Finite Elements

We use CFE for our simulations [HS97b, HS97a, HS98] and use the implementation of discretisation and solver for three-dimensional problems as described by [LPR+09, PRS07].

Table 1: Sample geometries ($3 \times 3 \times 3$ trabeculae) with diameter-to-length ratios (cf. Section 2.1) $d/l = (0.4, 0.4, 0.4)$ *(upper table)* and $d/l = (0.2, 0.2, 0.4)$ *(lower table)* are resolved at different resolution corresponding to 0.6/1.2 to 34.2/68.4 grid cells per trabecula. The tables show the computational resolution, the number of degrees of freedom used in the computation, the amount of memory used for storing the matrix of the system of equations and the total memory requirement for the simulation (also including object description, matrix, data vectors and multigrid solver). Results obtained at resolution 9^3 to 257^3 are compared to the 513^3 results, considering the fraction of volume segmented, and a root mean square (RMS) error of the displacement for compression and shear simulations, relative to the imposed displacement of 0.01.

Isotropic Diameters $d/l = (0.4, 0.4, 0.4)$

resolution	# DOF	matrix memory in MB	total memory in MB	volume fraction	RMS error (compression)	RMS error (shear)
9^3	1 665	0.88	5.06	0.883848	0.055986	0.027218
17^3	10 635	5.95	15.99	0.978967	0.015301	0.016932
33^3	55 365	36.51	78.78	0.992375	0.007203	0.011090
65^3	329 163	167.50	385.66	0.997552	0.003150	0.004636
129^3	2 227 491	770.87	2 121.34	0.999344	0.001287	0.001877
257^3	16 118 895	3 757.56	12 141.17	0.999868	0.000443	0.000561
513^3	122 019 597	20 211.29	79 944.99	1.0	0.0	0.0

Thin Transverse Diameters $d/l = (0.2, 0.2, 0.4)$

resolution	# DOF	matrix memory in MB	total memory in MB	volume fraction	RMS error (compression)	RMS error (shear)
9^3	1 395	0.88	4.52	0.841816	0.0401753	0.033242
17^3	8 163	5.94	14.50	0.978785	0.0175723	0.014527
33^3	39 789	33.27	70.07	0.992192	0.0066041	0.010219
65^3	213 309	148.69	343.03	0.997183	0.0029428	0.004587
129^3	1 358 175	677.20	1 926.19	0.999167	0.0014859	0.001654
257^3	9 562 185	3 360.91	11 341.66	0.999823	0.0006160	0.000510
513^3	71 219 541	18 606.01	76 716.81	1.0	0.0	0.0

CFE use degrees of freedom located on a uniform hexahedral grid consisting of cubes, effectively on the same grid on which the geometric shape of the elastic structure is described via a level set function [OS88]. Cubes are divided into six tetrahedra on which standard piecewise affine basis functions are adapted to CFE basis functions to reflect the actual domain boundary. The underlying uniform hexahedral grids contain canonical coarse scales, permitting to use the multigrid solver described in [LPR$^+$09].

2.3 Computational Resolution

As a preliminary simulation we consider two less complex samples ($3 \times 3 \times 3$ trabeculae without degradation; similar to [SWWR08]) over a wide range of resolutions (see Table 1). A relative root mean square error of less than 0.01 for the displacement in case of compression is obtained at 33^3 resolution, corresponding to 2.13 and 4.26 voxels per trabecular diameter for $d/l = 0.2$ and 0.4, respectively. Hence we consider computational grids with 129^3 nodes (corresponding to 5.12 and 2.56 voxels per trabecular diameter) sufficient for $10 \times 10 \times 10$ objects. For this resolution, our c++ CFE code can be run on a standard desktop PC.

2.4 Linearised Elasticity

As a description for linearised elasticity, we use the Lamé-Navier model with constants $\lambda = 9.779$ GPa and $\mu = 5.038$ GPa of the trabecular tissue. These correspond to a Young's modulus $E = 13.4$ GPa [RTP97], and according to the variations in [RTP97, LKHG98] we use a Poisson's ratio $\nu = 0.33$.

3 Results

Maximum loss of compressive stiffness of 89.8% is obtained for specimens with transverse isotropic diameters subjected to isotropic degradation. For shear, maximum loss of initial stiffness of 67.3% is reached for an isotropic structure subjected to isotropic degradation. Changing degradation from isotropic, to mainly transverse, to only transverse reduces the maximum loss of compressive stiffness from 76.6% to 50.3% to 6.3% for structures with trabecular diameter-to-length ratio (cf. Section 2.1) $d/l = (0.4, 0.4, 0.4)$ and from 89.8% to 66.5% to 2.1% for structures with $d/l = (0.2, 0.2, 0.4)$. In the shear case, the above changes reduce the maximum losses in stiffness from 67.3%, 52.1% to 35.8% for structures with $d/l = (0.4, 0.4, 0.4)$ and from 66.3% to 48.6% to 32.4% for structures with $d/l = (0.2, 0.2, 0.4)$ (Figure 1).

Varying the degradation from vertical direction over isotropic degradation to solely transverse isotropic degradation shows rising compressive stiffnesses from 748.61, 1421.56 to 1951.25 MPa for structures with $d/l = (0.4, 0.4, 0.4)$ and from 295.17, 939.01 to 1700.77 MPa for structures with $d/l = (0.2, 0.2, 0.4)$. For shear stiffness this leads to a lower change in stiffness from 123.60 to 159.35 to 173.57 MPa for structures with $d/l = (0.4, 0.4, 0.4)$ and from 31.14 to 40.97 to 44.24 MPa for structures with $d/l = (0.2, 0.2, 0.4)$. (Figure 2).

Keeping constant isotropic degradation ratios $(10\%, 20\%, 40\%)$ and varying $d/l \in [0.2, 0.7]$ for the transverse trabeculae shows an increase in stiffness 244.86%, 354.12% and 746.26% for thick transverse trabeculae compared to thin transverse trabeculae for the three degradation ratios respectively (Figure 3).

4 Discussion

The main advantage of CFE over classical FE is the representation of the geometric complexity of the specimen considered. By using uniform hexahedral grids (and treating the complicated shape in the basis functions), efficient data storage and cache-optimal data retrieval are achieved and all involved matrices have a uniform sparsity structure. Most importantly, geometric multigrid solvers can be used for efficient computations. Given the level set representation of the specimen, grid generation is a fully automatic and straightforward procedure and no global irregular tetrahedral meshing or artificial mesh smoothing is necessary.

The study shows the dependence of the structure stiffness on the degradation statistics of artificial lattice samples. The parameter study indicates that the worst drop of macroscopic compressive stiffness is obtained for a structure with transverse isotropic trabecular diameter under isotropic degradation of the trabeculae. The worst drop of shear stiffness is obtained for an isotropic structure under isotropic trabecular degradation with little difference to a transverse isotropic structure (Figure 1).

The loss of macroscopic compressive stiffness in case of isotropic degradation is presumably due to a loss in connectivity in all directions. This leads to lost support in loading direction as well as support through the bending stiffness of transverse trabeculae. Thinner transverse
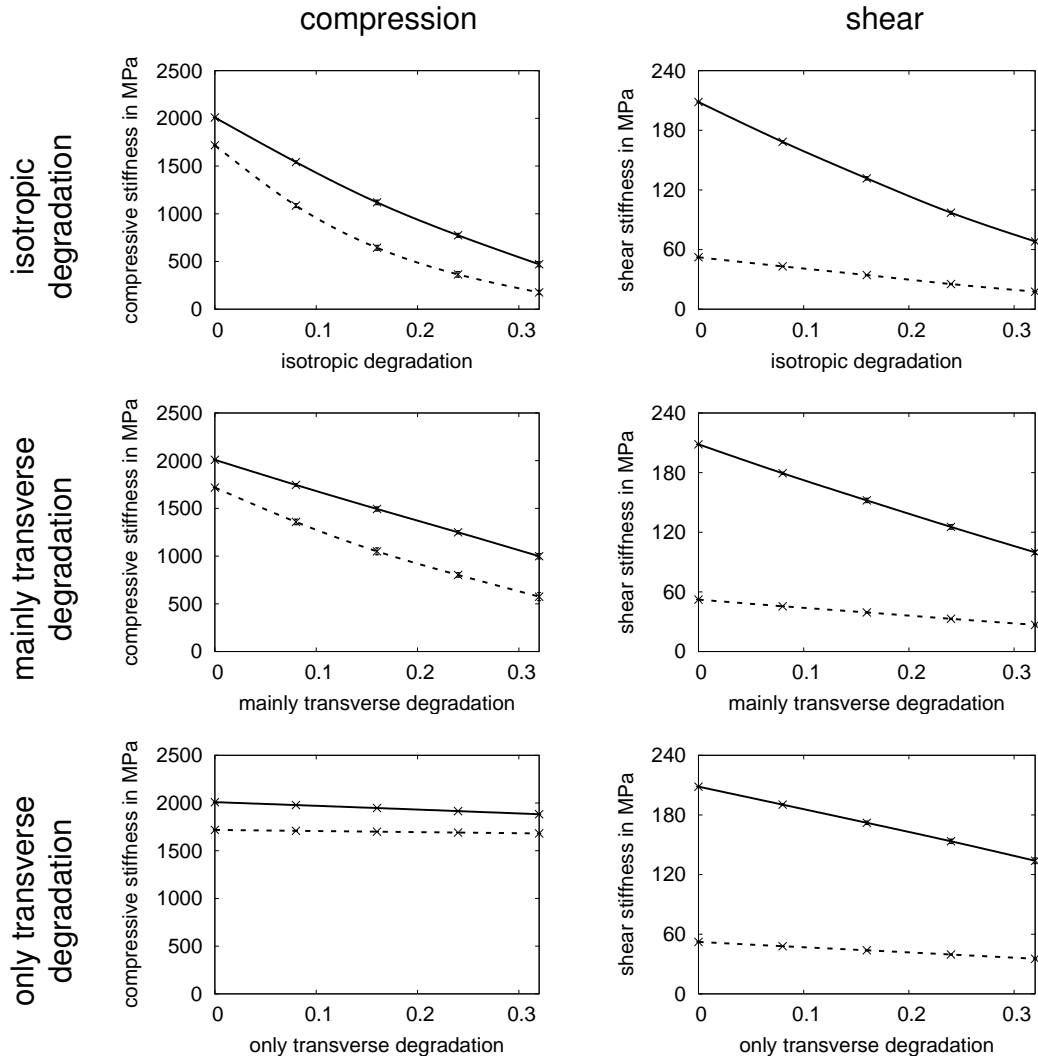
4

Figure 1: The plots show the stiffness in MPa for degradation ratios $\beta \in [0, 0.32]$ averaged over $n = 6$ samples along with the standard deviations. For samples with diameter-to-length ratios (cf. Section 2.1) $d/l = (0.4, 0.4, 0.4)$ *(solid lines)* and samples with diameter-to-length ratios $d/l = (0.2, 0.2, 0.4)$ *(dashed lines)*, we consider three different scenarios of trabecular loss: isotropic degradation (degradation ratios $p = (\beta, \beta, \beta)$, *top row*), degradation mainly in transverse directions ($p = (\beta, \beta, 0.5\beta)$, *middle row*) and degradation only in transverse directions ($p = (\beta, \beta, 0)$, *bottom row*). Results for uniaxial compression is shown in the left column, uniaxial shear in the right column.
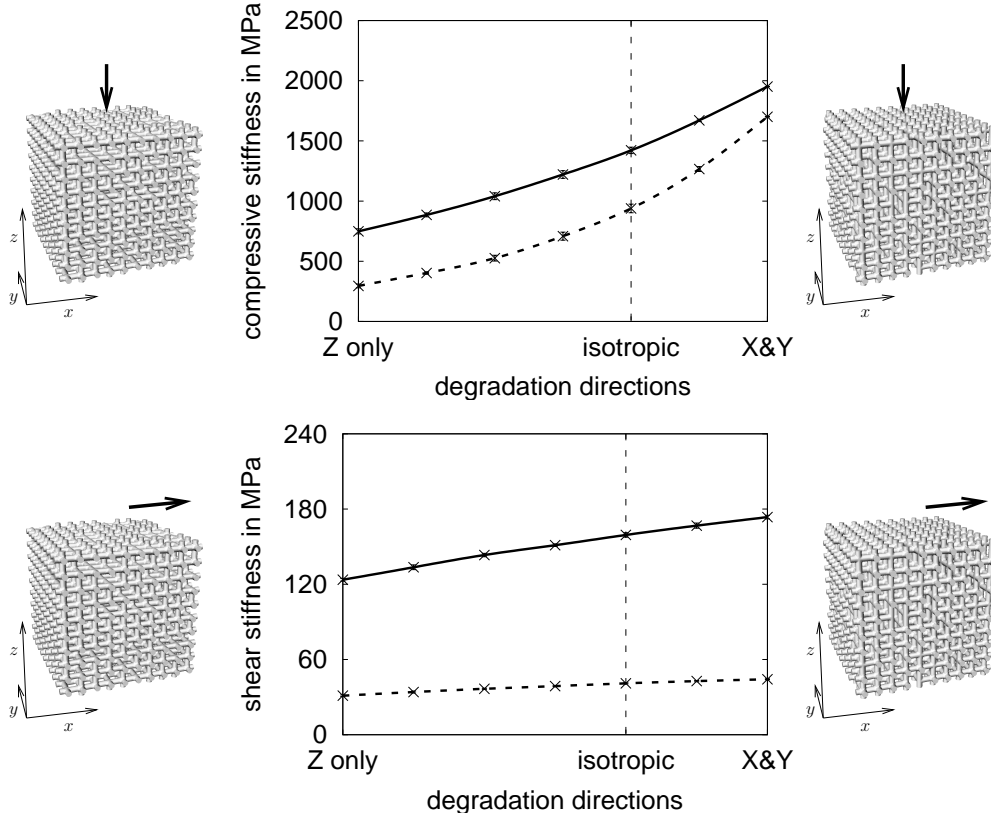
Figure 2: The plots show the stiffness in MPa averaged over $n = 6$ samples along with the standard deviations with varying degradation directions for uniaxial compression *(upper part)* and shear *(lower part)*. For two samples with isotropic diameters (diameter-to-length ratios (cf. Section 2.1) $d/l = (0.4, 0.4, 0.4)$, *solid lines*) and thinner diameters in the transverse directions ($d/l = (0.2, 0.2, 0.4)$, *dashed lines*) and a fixed overall degradation of 10% of the trabeculae, we vary the degradation anisotropy (degradation radios $p = (0.5\beta, 0.5\beta, 0.3 - \beta), \beta \in [0.0, 0.3]$) from degradation in longitudinal direction z only to isotropic degradation to degradation in transverse directions x and y only.
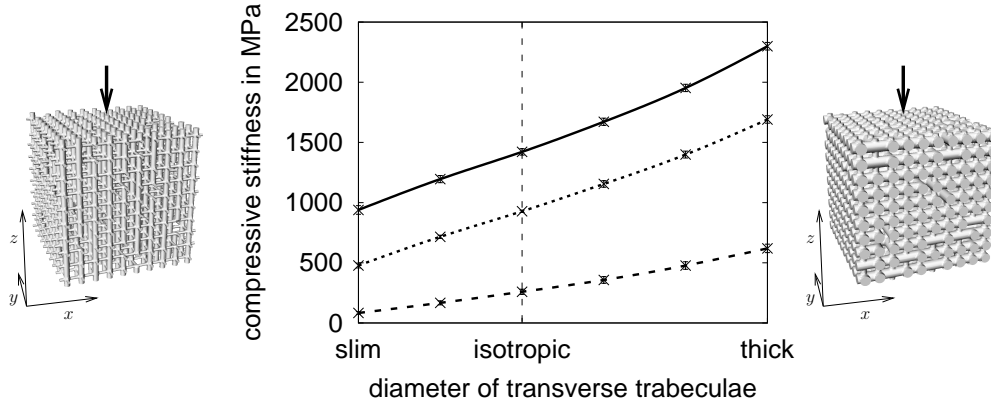
Figure 3: The plot shows stiffnesses in MPa averaged over $n = 6$ specimens along with the standard deviations for uniaxial compression. We consider isotropic degradation of 10% ($p = (0.1, 0.1, 0.1)$, cf. Section 2.1), *solid line*), 20% ($p = (0.2, 0.2, 0.2)$, *dotted line*) and 40% ($p = (0.4, 0.4, 0.4)$, *dashed line*) where the radius of the transverse trabeculae ($d/l = (\alpha, \alpha, 0.4), \alpha \in [0.2, 0.7]$) is varied from slim diameter in the transverse directions ($\alpha = 0.2$) to isotropic diameters ($\alpha = 0.4$) to thick diameter in the transverse directions ($\alpha = 0.7$).

trabeculae lead to a lower absolute stiffness (Figure 1). However, they have little influence on the relative loss of stiffness. Interestingly, degrading the structures solely transversely has little effect on the stiffness compared to isotropic degradation (Figure 1). This is more emphasised in Figure 2 where a variation of the degradation direction from loading direction to transverse direction reestablishes almost the initial stiffness.

Increasing the diameter of the transverse trabeculae results in rising macroscopic compressive stiffness due to an increased cross sectional area of vertical trabeculae (Figure 3).

Only simplified trabecular structures were used. While using real bone samples would have been more beneficial with respect to clinical questions, they are barely suitable for a rigorous parameter study. Our elasticity model is limited to linear elasticity as nonlinearities at microscopic level were not subject of this study.

Further work will include simulations for μCT-scanned samples of human vertebral trabecular bone. In order to determine the full tensor of elasticity for the artificial and natural samples described, a homogenisation procedure has been presented in [SWWR08]. Moreover, the concept of CFEs will be generalised to the case of multi-phase materials with discontinuous material parameter across geometrically complicated interfaces.

5 Acknowledgements

References

[BE92]   Marshall Bern and David Eppstein, *Computing in Euclidian geometry*, ch. Mesh generation and optimal triangulation, pp. 23–90, World Scientific, Singapore, 1992.

[BM06]   S. K. Boyd and R. Müller, *Smooth surface meshing for automated finite element model generation from 3D image data*, Journal of Biomechanics **39** (2006), no. 7, 1287–1295.

[BR02]   Achi Brandt and Dorit Ron, *Combinatorial optimization and vslicad*, ch. Multigrid Solvers and Multilevel Optimization Strategies, pp. 1–69, Kluwer Academic Publishers, 2002.

[Bra77]   Achi Brandt, *Multi-level adaptive solutions to boundary-value problems*, Mathematics of Computation **31** (1977), no. 138, 333–390.

[CPA+07] Y. Chevalier, D. Pahr, H. Allmer, M. Charlebois, and P. Zysset, *Validation of a voxel-based FE method for prediction of the uniaxial apparent modulus of human trabecular bone using macroscopic mechanical tests and nanoindentation*, Journal of Biomechanics **40** (2007), no. 15, 3333–3340.

[DSG05]   I. Diamant, R. Shahar, and A. Gefen, *How to select the elastic modulus for cancellous bone in patient-specific continuum models of the spine.*, Medical & Biological Engineering & Computation **43** (2005), no. 4, 465–472.

[DSMG07] I. Diamant, R. Shahar, Y. Masharawi, and A. Gefen, *A method for patient-specific evaluation of vertebral cancellous bone strength: in-vitro validation.*, Clinical Biomechanics **22** (2007), no. 3, 282–291.

[GK02]   X. E. Guo and C. H. Kim, *Mechanical consequence of trabecular bone loss and its treatment: a three-dimensional model simulation*, Bone **30** (2002), no. 2, 404–411.

[HJMH88] T. P. Harrigan, M. Jasty, R. W. Mann, and W. H. Harris, *Limitations of the continuum assumption in cancellous bone*, Journal of Biomechanics **21** (1988), no. 4, 269–275.

[HLM+99] T. Hildebrand, A. Laib, R. Müller, J. Dequeker, and P. Rüegsegger, *Direct three-dimensional morphometric analysis of human cancellous bone: Microstructural data from spine, femur, iliac crest and calcaneus*, Journal of Bone and Mineral Research **14** (1999), no. 7, 1167–1174.

[HS97a]   W. Hackbusch and S. A. Sauter, *Composite finite elements for problems containing small geometric details. Part II: Implementation and numerical results*, Computing and Visualization in Science **1** (1997), no. 1, 15–25.

[HS97b]   ———, *Composite finite elements for the approximation of PDEs on domains with complicated micro-structures*, Numerische Mathematik **75** (1997), no. 4, 447–472.

[HS98]   ———, *A new finite element approach for problems containing small geometric details*, Archivum Mathematicum **34** (1998), 105–117.

[KOJ05]   M. Karlsson, C. Obrant, and P. O. Josefsson, *Rockwood and green's fractures in adults*, ch. Fractures of Osteoporotic Bone, pp. 613–641, Lippincott Williams & Wilkins, 2005.

[LKHG98] A. J. Ladd, J. H. Kinney, D. L. Haupt, and S. A. Goldstein, *Finite-element modeling of trabecular bone: comparison with mechanical testing and determination of tissue modulus*, Journal of Orthopaedic Research **16** (1998), no. 5, 622–628.

[LPR+09] Florian Liehr, Tobias Preusser, Martin Rumpf, Stefan Sauter, and Lars Ole Schwen, *Composite finite elements for 3D image based computing*, Computing and Visualization in Science **12** (2009), no. 4, 171–188.

[MHR94]   R. Müller, T. Hildebrand, and P. Rüegsegger, *Non-invasive bone biopsy: a new method to analyse and display the three-dimensional structure of trabecular bone*, Physics in Medicine and Biology **39** (1994), 145–164.

[MM01]   R. Marcus and S. Majumdar, *Osteoporosis*, ch. The nature of osteoporosis., pp. 3–17, Academic Press, 2001.

[MYK05] E. F. Morgan, O. C. Yeh, and T. M. Keaveny, *Damage in trabecular bone at small strains*, European Journal of Morphology **42** (2005), no. 1, 13–21.

[OS88] S. J. Osher and J. A. Sethian, *Fronts propagating with curvature dependent speed: Algorithms based on Hamilton–Jacobi formulations*, Journal of Computational Physics **79** (1988), no. 1, 12–49.

[PRS07] Tobias Preusser, Martin Rumpf, and Lars Ole Schwen, *Finite element simulation of bone microstructures*, Proceedings of the 14th Workshop on the Finite Element Method in Biomedical Engineering, Biomechanics and Related Fields, University of Ulm, 2007, pp. 52–66.

[RSN⁺95] A. Randell, P. N. Sambrook, T. V. Nguyen, H. Lapsley, G. Jones, P. J. Kelly, and J. A. Eisman, *Direct clinical and welfare costs of osteoporotic fractures in elderly men and women.*, Osteoporosis International **5** (1995), no. 6, 427–432.

[RTP97] J.-Y. Rho, T. Y. Tsui, and G. M. Pharr, *Elastic properties of human cortical and trabecular lamellar bone measured by nanoindentation*, Biomaterials **18** (1997), no. 20, 1325–1330.

[She02] Jonathan Richard Shewchuk, *Delaunay refinement algorithms for triangular mesh generation*, Computational Geometry **22** (2002), no. 1-3, 21–74.

[SWWR08] Lars Ole Schwen, Uwe Wolfram, Hans-Joachim Wilke, and Martin Rumpf, *Determining effective elasticity parameters of microstructured materials*, Proceedings of the 15th Workshop on the Finite Element Method in Biomedical Engineering, Biomechanics and Related Fields, University of Ulm, July 2008, in press.

[TW00] Shang-Hua Teng and Chi Wai Wong, *Unstructured mesh generation: Theory, practice and applications*, International Journal of Computational Geometry & Applications **10** (2000), no. 3, 227–266.

[TWV⁺06] P. J. Thurner, P. Wyss, R. Voide, M. Stauber, M. Stampanoni, U. Sennhauser, and R. Müller, *Time-lapsed investigation of three-dimensional failure and damage accumulation in trabecular bone using synchrotron light*, Bone **39** (2006), no. 2, 289–299.

[vRHER03] B. van Rietbergen, R. Huiskes, F. Eckstein, and P. Rüegsegger, *Trabecular bone tissue strains in the healthy and osteoporotic human femur*, Journal of Bone Mineral Research **18** (2003), no. 10, 1781–1788.

[WWKL07] D. G. Woo, Y.-Y. Won, H.-S. Kim, and D. Lim, *A biomechanical study of osteoporotic vertebral trabecular bone: the use of micro-CT and high-resolution finite element analysis*, Journal of Mechanical Science and Technology **21** (2007), no. 4, 593–601.

[Xu89] Jinchao Xu, *Theory of multilevel methods*, PhD dissertation, Cornell University, May 1989.

[YK99] O. C. Yeh and T. M. Keaveny, *Biomechanical effects of intraspecimen variations in trabecular architecture : A three-dimensional finite element study*, Bone **25** (1999), no. 2, 223–228.